ELSEVIER

Alternative adsorption–desorption of C_3H_6 on nanotube-like silver titanate

Xiaodong Wang[a,b], Zhensheng Jin[b,*], Caixia Feng[b], Zhijun Zhang[b], Hongxin Dang[a,b,*]

[a]*Lanzhou Institute of Chemical Physics, Chinese Academy of Sciences, Lanzhou 730000, PR China*
[b]*Laboratory of Special Functional Materials, Henan University, Kaifeng 475001, PR China*

Abstract

A novel material—nanotube-like silver titanate (NST) was prepared from nanotube $H_2Ti_2O_4(OH)_2$ and characterized by means of TEM, XRD, XPS and DRS. Two kinds of alternative adsorption–desorption of C_3H_6 on NST were observed under visible light irradiation and in the dark. The deconvoluted alternative adsorption–desorption curve of C_3H_6 indicated that there exist two kinds of active sites on the surface of NST with quite different rates of adsorption and desorption. This phenomenon was discussed and explained.

© 2004 Elsevier Inc. All rights reserved.

Keywords: Nanotube-like silver titanate; Propylene; Alternative adsorption–desorption

1. Introduction

Nanotube $Na_2Ti_2O_4(OH)_2$, prepared by hydrothermal method, can be converted to nanotube $H_2Ti_2O_4(OH)_2$ when treated with a $0.1\,mol\,L^{-1}$ HCl solution [1]. After appropriate treatment, nanotube $H_2Ti_2O_4(OH)_2$ acquires some special properties, e.g., visible light absorption and emission [2–4], and it can be used in chromatographic separation of some homologous compounds [5], and also to improve optoelectronic characteristics of light-emitting diodes [6]. But nanotube $H_2Ti_2O_4(OH)_2$ exhibit poor activity in the photocatalytic removal of propylene [7].

When H^+ in nanotube $H_2Ti_2O_4(OH)_2$ exchanges with Ag^+, we can obtain nanotube-like silver titanate (NST). This novel material can absorb visible light and is expected to exhibit a photocatalytic property under visible-light irradiation. To our surprise, an alternative adsorption and desorption of C_3H_6 on NST occurs under visible-light irradiation and in the dark. The

deconvoluted adsorption–desorption curve shows that there exist two kinds of active sites (sites A and B) on NST surface. Under visible-light irradiation when C_3H_6 adsorbs on site $A(Ag^{m+})$, concurrently C_3H_6 desorbs from site $B(Ti^{n+})$, vice versa, in the dark when C_3H_6 adsorbs on site B, concurrently C_3H_6 desorbs from site A. Because of the great difference in the rates of the adsorption and desorption of C_3H_6, two types of alternative adsorption–desorption curves are formed. This phenomenon is discussed and explained herein.

2. Experimental

The preparation of nanotube $H_2Ti_2O_4(OH)_2$ was reported elsewhere [1]. An aqueous solution of $Ag(NH_3)_2^+$ was prepared by the reaction of $10.0\,M$ $AgNO_3$ solution with aqueous ammonia at room temperature [8]. After the addition of a few drops of aqueous ammonia, a brown precipitate appeared and then an additional amount of aqueous ammonia was added slowly to dissolve the precipitate until a clear $Ag(NH_3)_2^+$ solution was produced. Nanotube of $1.6\,g$ of $H_2Ti_2O_4(OH)_2$ and $30\,ml$ of $Ag(NH_3)_2^+$ solution were

*Corresponding author. Tel.: +86 378 2192331;
fax: +86 378 2867282.

E-mail address: zhenshengjin@henu.edu.cn (Z. Jin).

added into a round-bottom flask and refluxed for 24 h at 60 °C, then filtered, washed with distilled water to neutral, and dried under vacuum at room temperature, a yellow powder NST was obtained. The content of Ti of this powder was determined by the colorimetric method on a UNICAM HEλIOSα UV-Vis absorption spectrometer, and the content of Ag was analyzed on a Hitachi 180-60 atomic absorption spectrometer.

Transmission electron microscopic (TEM) images and energy-dispersive X-ray analysis (EDX) were taken on a JEM-2010 electron microscope, the spot size for EDX analysis = 10 nm. The X-ray diffraction (XRD) spectra were obtained on a Philips X' Pert Pro X-ray diffractometer with monochromatized Cu$K\alpha$ radiation ($\lambda = 1.5406$ Å). Spectra of X-ray photoelectron spectroscopy (XPS) and Auger electron spectroscopy (AES) were recorded on an AXIS ULTRA X-ray photoelectron spectrometer (KRATOS ANALYTICAL Ltd., UK). The relative atomic concentrations of NST surface were calculated on a computer using a XPS sensitivity factor. UV-Vis diffuse reflectance spectra (DRS) were obtained on a UV-2100 spectrometer.

The experimental equipment is shown in Fig. 1. NST powder of 23 mg was spread on one side of a roughened glass plate located in a flat quartz tube reactor. The visible-light source was a 500 W Xenon lamp, which was kept at a distance of 330 mm to the reactor. Between the Xenon lamp and the reactor, a $\lambda = 420$ nm cut filter and a water cell were inserted to eliminate the UV and infrared light, respectively. The feed gas was made up of pure C_3H_6 (99.9%) and Ar (99.99%), and was stored in a high-pressure cylinder. The concentration of C_3H_6 was determined by a chromatographic method (on a Shimadzu GAS CHROMATOGRAPH GC-9A with a hydrogen flame detector, in situ analysis, time interval for each analysis is 5 min). The sensitivity of the analysis

for C_3H_6 was 1 ppmv. C_0 (C_3H_6 concentration of feed gas) was equal to 573 ppmv, corresponding to $0.22\ \mu mol \cdot mL^{-1}$. C denoted the C_3H_6 concentration outlet of reactor ($\mu mol \cdot mL^{-1}$). The flow rate of the feed gas (R) was 97 mL $\cdot$ min^{-1}. The adsorption/desorption rate(V) = $(C_0 - C)/C_0 \times R$ ($\mu mol \cdot min^{-1}$).

3. Results and discussion

Fig. 2a–d show the TEM images of nanotube $H_2Ti_2O_4(OH)_2$ and Ag$^+$ ion-exchanged nanotube $H_2Ti_2O_4(OH)_2$ (i.e., NST), respectively. After the replacement of H$^+$ in nanotube $H_2Ti_2O_4(OH)_2$ by Ag$^+$, a great number of clusters (ca. 2–5 nm sized) are formed and they have a nanotube-like structure (Fig. 2c,d). The chemical state of Ag in NST was determined by the X-ray excited AES. The chemical shift of AES peak of AgM4VV varies in the range of a few electron volts, but the XPS Ag3$d_{5/2}$ peak is almost not affected by the chemical environment. Fig. 3 and Table 1 show that the binding energy E_b(AgM4VV) is 1131.0 eV. Since the X-ray radiation source Al $K\alpha$ is 1486.6 eV, the kinetic energy, E_k(AgM4VV), is 355.6 eV(1486.6–1131.0 eV), which corresponds to Ag$^+$. If it were Ag^0, E_k(AgM4VV) would be 358.0 eV [9]. From E_b(Ag3$d_{5/2}$) = 368.7 eV (Fig. 3a), we cannot distinguish the chemical states of Ag [9]. E_b(Ti2$p_{3/2}$) and E_b(O1s) of both NST and nanotube $H_2Ti_2O_4(OH)_2$ are the same (Fig. 4a–d and Table 1). E_b(Ti2$p_{3/2}$) = 459.0 eV, corresponds to Ti^{4+} while E_b(O1 s) = 530.4 and 531.8 eV, corresponds to O^{2-} and OH$^-$, respectively [9]. The surface Ag/Ti atomic ratio calculated from ESCA results is equal to 0.6, which is close to that obtained by chemical analysis (0.5) (Table 1). Therefore, we assume the empirical formula of NST to be AgHTi$_2$O$_4$(OH)$_2$. Here a question is posed: what is the reason that many clusters form and constitute a nanotube-like structure? Fig. 2d shows that after the exchange of H$^+$ with Ag$^+$ ion, parts of nanotubes are destroyed to form clusters, while the undestroyed parts still remain its layered structure but slightly zigzagged. At the undestroyed parts, the distance between two adjacent layers is 0.7 nm (Fig. 2d) slightly less than that of $H_2Ti_2O_4(OH)_2$ nanotube 0.8 nm (see Fig. 2b). The EDX results (Table 2) show that at different locations in Fig. 2c, the Ag/Ti atomic ratios are not identical, i.e. 0.49, 0.55, 0.44, 0.46 and 0.47, respectively, and the average value is equal to 0.48, which is close to both ESCA and chemical analysis results. The variations in composition and morphology reveal that the exchange rates of H$^+$ with Ag$^+$ ion at the different parts of $H_2Ti_2O_4(OH)_2$ nanotube are different, which is possibly resulted from the different diffusion rates of Ag$^+$ ions into nanotube structure. The Ag$^+$ ion-exchanged parts would coagulate to produce a new phase (i.e., clusters).
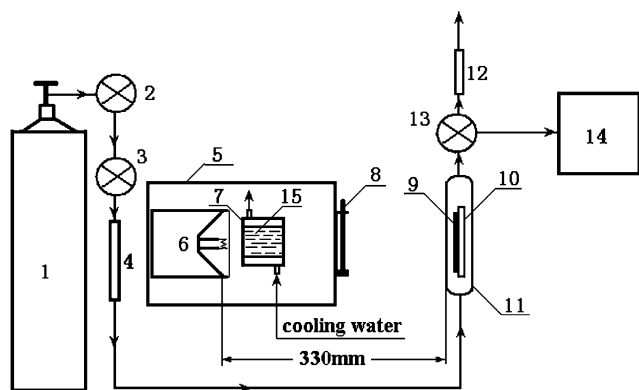

Fig. 1. Experimental equipment (1) feed gas cylinder; (2) gas regulator; (3) gas reset valve; (4) drying-tube (filled with anhyrous magnesium perchlorate); (5) chamber; (6) Xenon lamp; (7) water cell; (8) filter (420 nm); (9) catalyst; (10) glass plate; (11) quartz reactor; (12) soap film flowmeter; (13) six-way valve; (14) gas chromatograph; (15) distilled water.
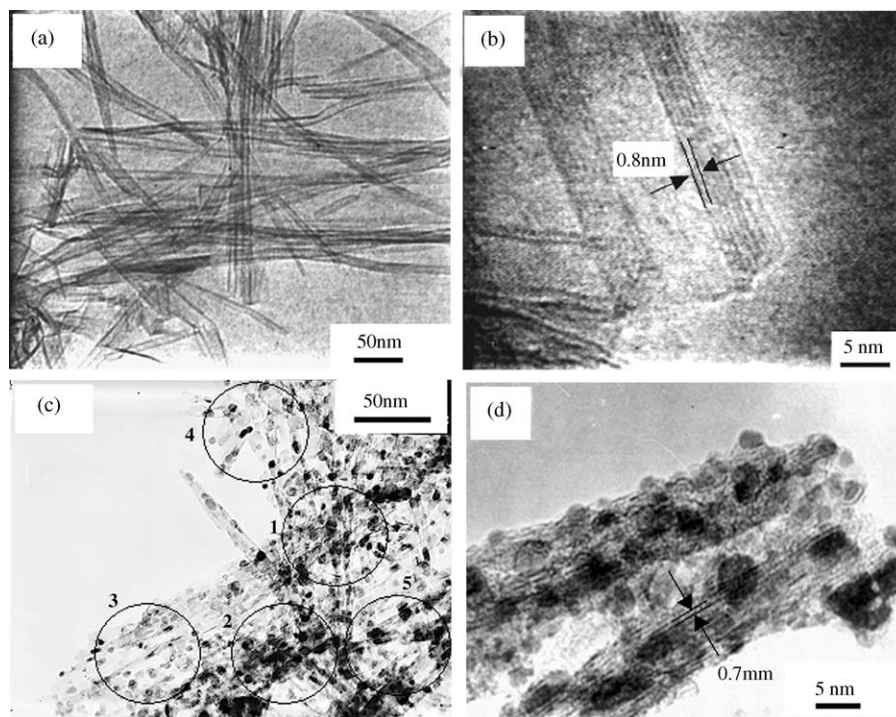
Fig. 2. TEM images of nanotube $H_2Ti_2O_4(OH)_2$ (a,b) and Ag^+ ion-exchanged nanotube $H_2Ti_2O_4(OH)_2$ (c,d).
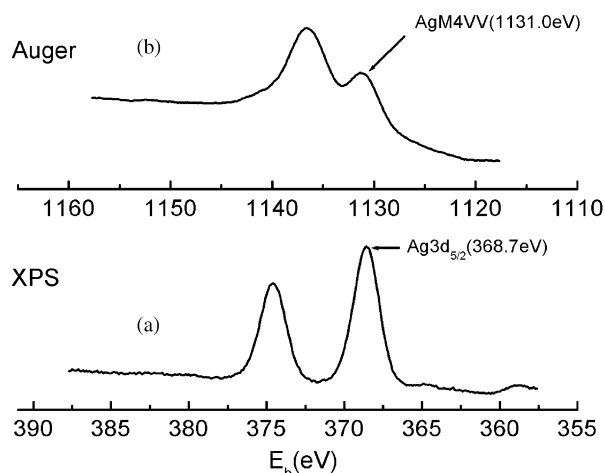
Fig. 3. XPS and AES spectra of Ag^+ ion-exchanged nanotube $H_2Ti_2O_4(OH)_2$: (a) Ag3d; (b) Ag(MVV).

These clusters are arranged along the axial direction of the original nanotubes(Fig. 2c), so they constitute a nanotube-like material.

Fig. 5a shows the XRD pattern of nanotube $H_2Ti_2O_4(OH)_2$, which belongs to an orthorhombic system with poor crystallinity [1,10–11]. The XRD pattern of NST (Fig. 5b) is different from that of nanotube $H_2Ti_2O_4(OH)_2$(Fig. 5a): peaks $200(2\theta = 9.18°)$, $110(2\theta = 24.30°)$ and $600(2\theta = 28.14°)$ disappear;

three unknown peaks($2\theta = 29.10°$, $34.83°$ and $37.37°$) emerge, which are not the peaks of $(I/I_0)_{100}$ (Ag) [11], $(I/I_0)_{100}$ (Ag_2O)[12] or $(I/I_0)_{100}$ (AgO)[13]. According to above discussion for the composition and morphology of NST, Fig. 5b represents the pattern of a composite, not of a single compound, so it cannot give us a complete information about the crystal structure of NST. But three unknown peaks must correlate with the existence of Ag^+ ion-exchange parts in NST. DRS spectra indicate that NST has distinct absorption at $\lambda > 420$ nm (Fig. 6b), but nanotube $H_2Ti_2O_4(OH)_2$ has no response to visible light (Fig. 6a).

On NST we obtained two special types of C_3H_6 adsorption–desorption curves (Fig. 7a): under visible light irradiation, desorption of C_3H_6 takes place first, then transforms to adsorption of C_3H_6 until $V = 0$; in the dark, adsorption of C_3H_6 takes place first, then transforms to desorption of C_3H_6 until $V = 0$. Such alternative C_3H_6 adsorption–desorptions repeat for many times. In Fig. 7a, six runs are illustrated, three under visible light irradiation, and three in the dark. However, no adsorption of C_3H_6 are observed on nanotube $H_2Ti_2O_4(OH)_2$ both under visible light irradiation and in the dark (Fig. 7b). Therefore, we can conclude that the alternative C_3H_6 adsorption–desorptions take place on Ag^+ ion-exchanged parts of nanotube.

How to explain the phenomena of alternative C_3H_6 adsorption–desorption on NST? It is known that under

Table 1
XPS and AES analysis for $H_2Ti_2O_4(OH)_2$ and Ag^+ ion-exchanged product

Samples	O1s E_b (eV)		Ti $2p_{3/2}$ E_b(eV)	Ag $3d_{5/2}$ E_b(eV)	AgM4VV E_k(eV)	Ag/Ti* atomic ratio
$H_2Ti_2O_4(OH)_2$	530.4	531.8	459.0	—	—	0
Ag^+ ion-exchanged product	530.3	531.8	458.9	368.7	355.6	0.6

*Chemical analysis results: Ag(mass)% = 39.4, Ti(mass)% = 34.78, Ag/Ti(atomic) = 0.5.
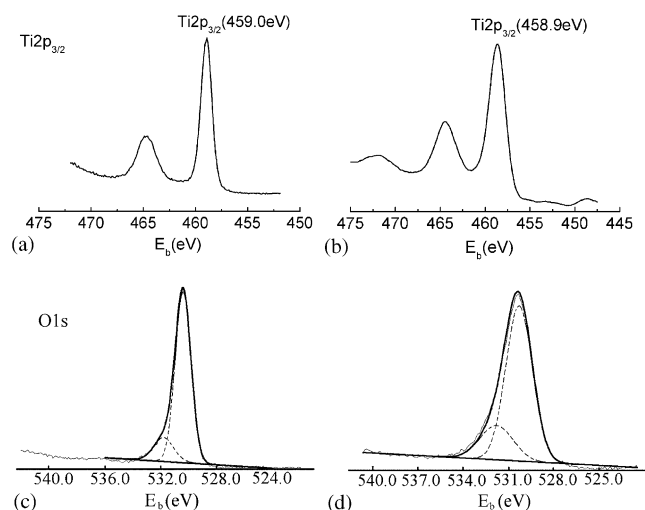
Fig. 4. XPS spectra: (a) Ti2p of nanotube $H_2Ti_2O_4(OH)_2$;(b)Ti2p of NST; (c)O1s of nanotube $H_2Ti_2O_4(OH)_2$;(d)O1s of NST.

constant test conditions, adsorption and desorption of C_3H_6 cannot take place on an identical surface site in sequence. So we propose that there exist two kinds of surface active sites (sites A and B) on NST. Under visible-light irradiation when C_3H_6 is adsorbed on site A, C_3H_6 simultaneously desorbed from site B, however, in the dark when C_3H_6 is adsorbed on site B, C_3H_6 simultaneously desorbed from site A. Due to the great difference between the rates of adsorption and desorption, the net rate curve is in an alternative adsorption–desorption form. The deconvolution of curve run 1 was carried out on a computer (Fig. 8), where the solid line represents the experimental result, and the dash line—deconvoluted result, positive V denotes the adsorption rate (i.e., V_a, in μmol min^{-1}), and negative V denotes the desorption rate (i.e., V_d, in μmol min^{-1}). According to the Langmuir rate theory [14]:

$$V_a = \alpha \frac{P}{\sqrt{2\pi mkT}}(1-\theta^A)e^{-E_a/(RT)} = a(1-\theta^A)e^{-E_a/(RT)},$$
(1)

$$V_d = bf'(\theta)e^{-E_d(\theta)/(RT)},$$
(2)

where α, a, b are the constants, P the partial pressure of C_3H_6 in the feed gas, m the molecular weight of C_3H_6, k

is Boltzmann constant, T is absolute temperature, θ^A is coverage of C_3H_6 on site A, θ^B is coverage of C_3H_6 on site B, E_a is activation energy of C_3H_6 adsorption, E_d is the activation energy of C_3H_6 desorption.

Assuming that the activation energy changes linearly with the coverage of C_3H_6, then

$$E_a = E_a^0 + \delta\theta^A,$$
(3)

$$E_d = E_d^0 - \eta\theta^B,$$
(4)

$$V_a = a(1-\theta^A)e^{-E_a^0/RT}e^{-\delta\theta^A/(RT)} = a'(1-\theta^A)e^{-\delta\theta^A/(RT)},$$
(5)

$$V_d = b\theta^B e^{-E_d^0/RT} \cdot e^{\eta\theta^B/(RT)} = b'\theta^B \cdot e^{\eta\theta^B/(RT)}.$$
(6)

θ^A can be obtained from the deconvoluted curve shown in Fig. 8. $(S^A)_{t=t(final)}$ is the total area covered by the deconvoluted curve of site A at $t = t_{final}$, $(S^A)_{t=t}$ is the area covered by the deconvoluted curve of site A at time t, then

$$\theta^A = (S^A)_{t=t}/(S^A)_{t=t(final)},$$
when $t = 0$, $(S^A)_{t=0} = 0$, $\theta^A = 0.$
(7)

Similarly,

$$\theta^B = [(S^B)_{t=t(final)} - (S^B)_{t=t}]/(S^B)_{t=t(final)},$$
when $t = 0$, $(S^B)_{t=0} = 0$, $\theta^B = 1.$
(8)

According to deconvoluted curves of run 1, we can plot $\ln[V_a/1 - \theta^A)]$ vs. θ^A, and $\ln(V_a/\theta^B)$ vs. θ^B. Fig. 9a and b show that there are two straight lines. Using the slopes and intercepts we obtain two equations:
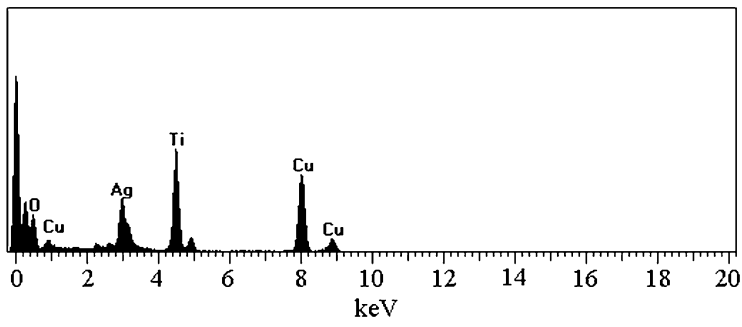
$$V_a = 0.121(1 - \theta^A)e^{1.33\theta^A},$$
(9)

$$V_d = 1.44\,\theta^B e^{-2.77\theta^B}.$$
(10)

The apparent rate constant of V_d(1.44) is about one order magnitude larger than that of V_a(0.121). The above-mentioned calculations confirm that curve run 1 is a superposition of C_3H_6 adsorption curve on site A and C_3H_6 desorption curve on site B. Using the same procedure, we can also confirm that curve run 2 is a superposition of C_3H_6 adsorption curve on site B and C_3H_6 desorption curve on site A.

Undoubtedly, the different C_3H_6 adsorption–desorption properties of sites A and B are correlated with the

Table 2
EDX results for NST at different locations in Fig. 2c

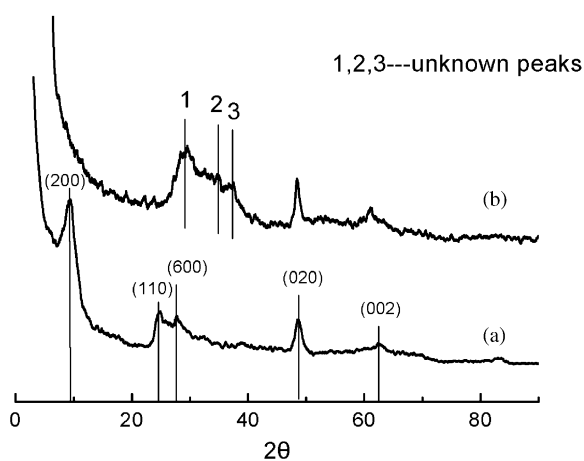| Location	Ag/Ti atomic ratio	Typical spectrum
1	0.49	
2	0.55	
3	0.44	
4	0.46	
5	0.47	
Average	0.48	

Note: Cu peaks are attributed to Cu grid.

Fig. 5. XRD patterns of nanotube $H_2Ti_2O_4(OH)_2$(a) and NST (b); peak1, peak2 and peak3 are the three unknown peaks.
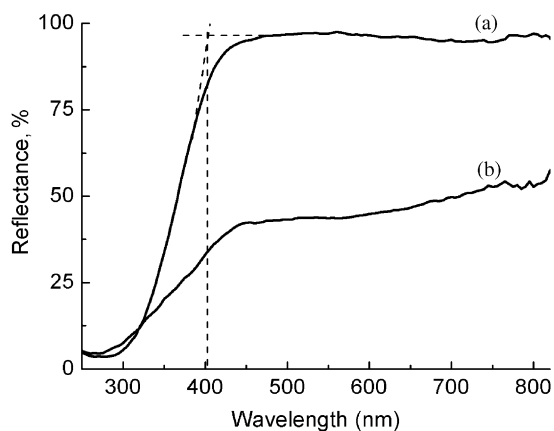
Fig. 6. DRS of nanotube $H_2Ti_2O_4(OH)_2$ (a) and NST (b).

chemical nature of Ag^+ ion-exchanged parts of nanotube. Kato et al. reported that Ag4d and O2p orbitals can hybridize to form a valence band of $AgMO_3$ ($M = V, Ta$) and the energy level of the hybrid orbitals is 0.6 eV positive than that of O2p [15,16]. From the results shown in Fig. 6a,b, it can be seen that when nanotube $H_2Ti_2O_4(OH)_2$ is converted to nanotube-like $Ag_xH_{2-x}Ti_2O_4(OH)_2$ ($x \approx 1$), the visible-light response appears. So we infer that in NST the hybridization of Ag4d and O2p orbitals also takes place, so that the E_g(band gap) of NST is less than that of nanotube $H_2Ti_2O_4(OH)_2$ (Fig. 10). Ti^{n+} has a smaller ionic radius (assuming that Ti^{n+} is site B, $r_{Ti(IV)} = 0.60$ Å for coordination number 6) with more positive charges than Ag^{m+}(assuming Ag^{m+} is site A, $r_{Ag(I)} = 1.10$ Å for coordination number 6) [17]. Alkenes are nucleophilic reagents [18]. In the dark, NST is in the ground state and the nucleophilic molecule C_3H_6 would adsorb on the surface of Ti^{n+} but not on the surface of Ag^{m+}. When the valence-band electron is excited to the conduction band under visible-light irradiation, a negative charged center would be generated on the surface of Ti^{n+} while simultaneously a positive charged center would be formed on the surface of Ag^{m+}. In the circumstance, C_3H_6 would adsorb on the surface of Ag^{m+} while C_3H_6 originally adsorbed on the surface of Ti^{n+}, would simultaneously desorb with a much larger rate than that of C_3H_6 adsorption on Ag^{m+}. For this reason, two special types of C_3H_6 adsorption–desorption curves under visible light irradiation and in the dark are obtained (Fig. 7a). The reason why no adsorption C_3H_6 appeared on nanotube $H_2Ti_2O_4(OH)_2$ both under visible light irradiation and in the dark(Fig. 7b) may be resulted from the difference of the electronic configuration between $H_2Ti_2O_4(OH)_2$ and Ag^+ ion-exchanged $H_2Ti_2O_4(OH)_2$.

Alternative adsorption–desorption of the nucleophilic substance on NST may induce the alternative change of surface properties of NST, e.g., electric property. Our further study is to explore the application of this novel material.
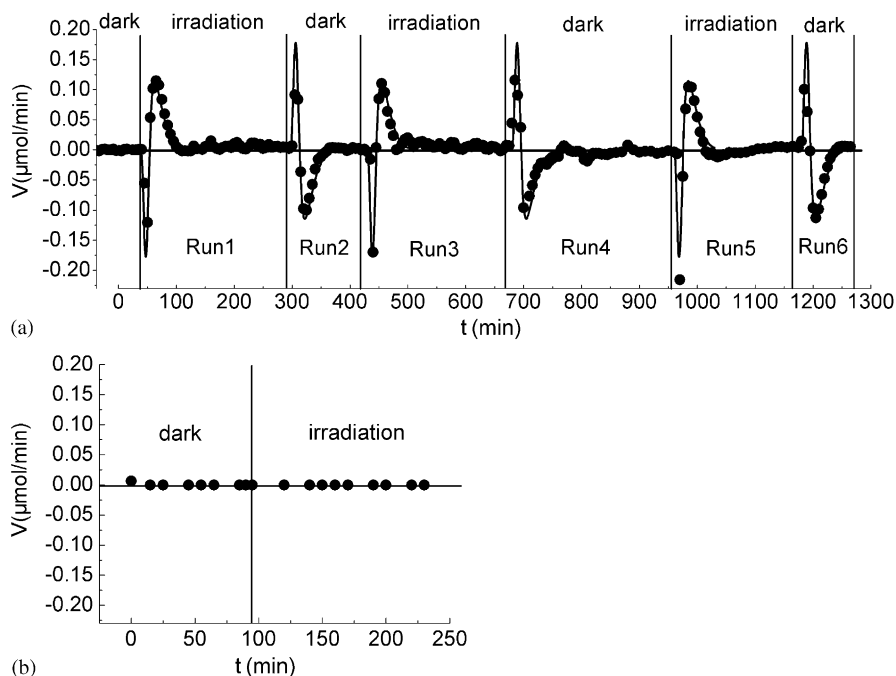
Fig. 7. Adsorption–desorption curves of C_3H_6: (a) on NST(time interval of analysis = 5 min); (b) on nanotube $H_2Ti_2O_4(OH)_2$.
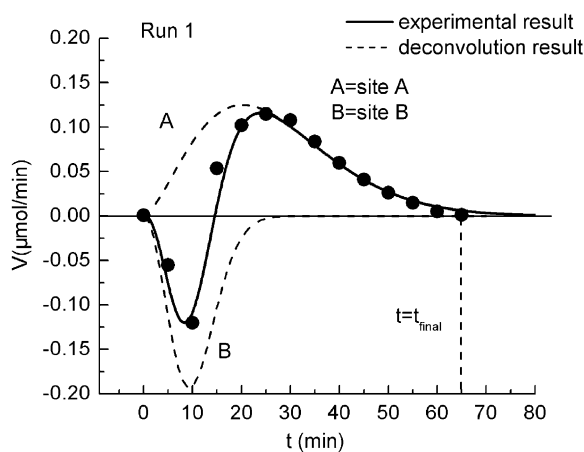

Fig. 8. Deconvoluted curve of Run 1.

Fig. 9. Dependence of $\ln(V/(1 - \theta^A))$ on θ^A (a) and dependence of $\ln(V/\theta^B)$ on θ^B (b).

4. Conclusion

A novel material—nanotube-like silver titanate was prepared by an ion-exchange method and was characterized by means of TEM, XRD, XPS and DRS. There exist two kinds of C_3H_6 adsorption sites (Ti^{n+} and Ag^{m+}) on the surface of nanotube-like silver titanate. In the dark, C_3H_6 adsorbs on Ti^{n+}, and simultaneously desorbs from Ag^{m+}. Under visible-light irradiation, C_3H_6 adsorbs on Ag^{m+}, and simultaneously desorbs from Ti^{n+}. Due to the great difference between the rates of adso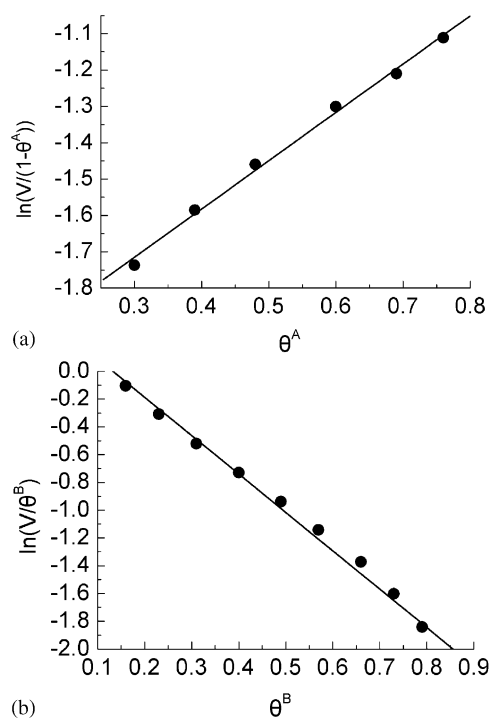rption and desorption, an alternative adsorption–desorption of C_3H_6 on nanotube-like silver titanate occurs both under visible-light irradiation and in the dark.

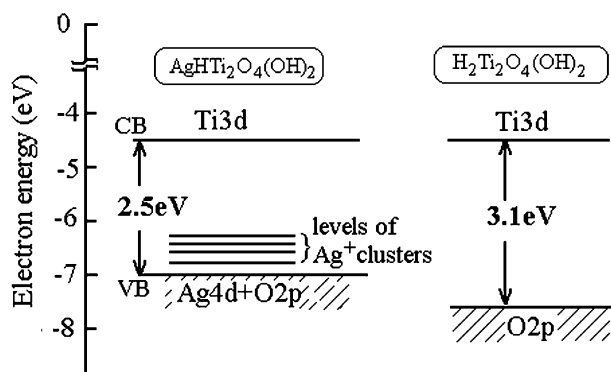Fig. 10. Schematic diagram of band structure of NST and nanotube $H_2Ti_2O_4(OH)_2$.

Acknowledgments

References

[1] Jianjun Yang, Zhensheng Jin, Xiaodong Wang, Wei Li, Jingwei Zhang, Shunli Zhang, Xinyong Guo, Zhijun Zhang, Dalton Trans. 20 (2003) 3898–3901.

[2] Shunli Zhang, Wei Li, Zhensheng Jin, Jianjun Yang, Jingwei Zhang, Zuliang Du, Zhijun Zhang, J. Solid State Chem. 177 (2004) 1365–1371.

[3] L. Qian, Z.S. Jin, J.W. Zhang, Y.B. Huang, Z.J. Zhang, Z.L. Du, Appl. Phys. A, in press.

[4] Wei Li, Zhensheng Jin, Jianjun Yang, Zhijun Zhang, Photographic Sci. Photochem. (Chinese) 21 (2003) 273–279.

[5] Zhao Guohong, Li Wei, Wang Zhonglai, Wang Hanqing, Yang Jianjun, Chen Lireng, J. Anal. Chem. (Chinese) 32 (2004) 299.

[6] L. Qian, F. Teng, Z.S. Jin, Z.J. Zhang, T. Zhang, Y.B. Hou, S.Y. Yang, X.R. Xu, J. Phys. Chem. B 108 (2004) 13928–13931.

[7] Ming Zhang, Zhensheng Jin, Jingwei Zhang, Xinyong Gao, Jianjun Yang, Wei Li, Xiaodong Wang, Zhijun Zhang, J. Mol. Catal. A: Chem 217 (2004) 203.

[8] Sofian M. Kanan, Marsha C. Kanan, Howard H. Patterson, J. Phys. Chem. B 105 (2001) 7508–7516.

[9] C.D. Wagner, W.M. Riggs, L.E. Davis J.F. Moulder, G.E. Muilenberg (Ed.), Handbook of X-ray Photoelectron Spectroscopy, Perkin-Elmer Corporation, Eden Prairie, MN, 1979.

[10] M. Sugita, M. Tsuji, M. Abe, Bull. Chem. Soc. Jpn. 63 (1990) 1978–1984.

[11] Joint Committee on Powder Diffraction Standard, 87–0720.

[12] Joint Committee on Powder Diffraction Standard, 76–1393.

[13] Joint Committee on Powder Diffraction Standard, 76–1489.

[14] A.W. Adamson, A.P. Gast, Physical Chemistry of Surfases, Sixth ed, Wiley, New York, 1997.

[15] Hideki Kato, Hisayoshi Kobayashi, Akihiko Kudo, J. Phys. Chem. B 106 (2002) 12441–12447.

[16] Ryoko Konta, Hideki Kato, Hisayoshi Kobayashi, Akihiko Kudo, Phys. Chem. Chem. Phys. 5 (2003) 3061–3065.

[17] A. John Dean, Lange's Handbook of Chemistry, 15th ed, McGraw-Hill, New York, 1999.

[18] I.L. Finar, Organic Chemistry, sixth ed, vol. 1, Longman, New York, 1973, p. 102.